

1 A hit-and-run Giant Impact scenario

2 Andreas Reufer¹, Matthias M. M. Meier^{2,3}, Willy Benz¹ and Rainer Wieler²

3 ¹ Physikalisches Institut & Center for Space and Habitability, Universität Bern, Sidlerstrasse 5, 3012 Bern, Switzerland

4 ² Institut für Geochemie und Petrologie, Eidgenössische Technische Hochschule Zürich, Clausiusstrasse 25, 8092
5 Zürich, Switzerland

6 ³ Department of Geology, Lund University, Sölvegatan 12, 22362 Lund, Sweden

7

8 *Abstract*

9 *The formation of the Moon from the debris of a slow and grazing giant impact of a Mars-sized*
10 *impactor on the proto-Earth (Cameron & Ward 1976, Canup & Asphaug 2001) is widely accepted*
11 *today. We present an alternative scenario with a hit-and-run collision (Asphaug 2010) with a*
12 *fractionally increased impact velocity and a steeper impact angle.*

13

14 1. **Introduction**

15 Hydrodynamical simulations have identified a slow, grazing impact in being able to reproduce the
16 Moon's iron deficiency and the angular momentum of the Earth-Moon-system. But in this canonical
17 scenario, the Moon forms predominantly from impactor material, thus contradicting the Moon's
18 close geochemical similarity to Earth. Furthermore, due to the slow impact velocity, only limited
19 heat input is provided for the aftermath of the collision. Post-impact mechanisms (Pahlevan &
20 Stevenson 2007) required to match the impact scenario with the compositional observations,
21 depend on the thermal conditions in the post-impact debris disk. We show that a new class of hit-
22 and-run collisions with higher impact velocities and a steeper impact angles is also capable of
23 forming a post-impact debris disk from which the Earth's Moon can later form, but leads to a much
24 hotter post-impact debris disk. Furthermore, the ratio of target body material in the debris disk is
25 considerably larger, compared to the canonical scenario. This new class of impacts was previously

26 rejected due to the limited resolutions of early simulations (Benz 1989).

27

28 2. **Methods**

29 We use a 3D SPH code with self-gravity but without strength (Reufer 2011) similar to previous
30 work modelling the Giant impact (Benz 1989, Canup & Asphaug 2001). Smoothed Particle
31 Hydrodynamics (Monaghan 1992) represents matter in a Lagrangian way by representing mass as
32 individual particles. This allows to track not only the type of material but also the origin of the
33 material. For the equation of state, we use ANEOS (Thompson & Lauson 1972) for iron and water
34 ice, and M-ANEOS (Melosh 2007) for the silicate layers composed of quartz.

35 Initial target and impactor are set up, by starting with isentropic vertical profiles for desired masses
36 and composition. The physical quantities of those profiles like density and specific energy are then
37 mapped onto spheres of SPH particles. These spheres are relaxed until the residual particle
38 velocities fall below 1% of the body's escape velocity, the latter being on the order of magnitude of
39 the impact velocity. Individual simulations are then setup by placing relaxed spheres onto the orbit
40 required for a collision with the desired impact angle and velocity and setting the initial velocity
41 vectors accordingly. The total number of particles in the simulations varies between 500k to 550k,
42 so that a post-impact disk of a Moon mass is represented by roughly 10k particles. This is similar to
43 recent high-resolution simulations of the giant impact and good enough to determine the
44 composition and thermal state of the post-impact disk.

45 Simulations are post-processed the same way as in previous work (Benz et al. 1986, Canup &
46 Asphaug 2001, Canup et al. 2001, Canup 2004, Canup et al. 2012): First the particles of the central
47 body are found with the following algorithm: Particles near the center of mass of all particles are
48 taken as a first guess for the central body. New particles are added to the existing body, if they are
49 gravitationally bound to it, but not in an orbit around it. The surface of the central body is then
50 given by the particles, which have a density near the zero-pressure density of the material. For the

51 remaining particles the orbits are then determined relative to the central body. If the periapsis lies
52 above the central body's surface and the orbit is closed, a particle is considered a part of the debris
53 disk. Otherwise particles are either re-impacting the central body or escaping the system.
54 While in the canonical case, the orbital time scale of the material in the debris disk is on the order
55 of only a few hours, the increase in impact velocity in our simulations also leads to an increase in
56 the orbital time scale of the disk material. Therefore we integrate the simulations to roughly 50h
57 after the actual impact.

58

59 3. **Theory**

60 The collisional parameters for the giant impact considered so far have, however, been limited to
61 low-velocity collisions at or only slightly above mutual escape velocity between target and
62 impactor. The Earth-Moon system is not believed to have lost more than 10% of its initial angular
63 momentum between the giant impact and today (Canup et al. 2001). In low-velocity collisions, very
64 little mass and therefore also very little angular momentum is lost, compared to the total mass and
65 angular momentum before the collision. Hence if impact velocity and angular momentum of the
66 collision are fixed values, for a given impactor and target composition only one degree of freedom
67 remains in the form of the product of the sine of impact angle and the impactor mass. Previous
68 work therefore focussed on finding the optimum mass ratio between impactor and target. Recent
69 work suggests a mass ratio of 9:1 and a total mass of $1.05 M_E$ (Canup 2004). Both the impactor and
70 the target are assumed to be differentiated bodies with a 30wt% iron core and a 70wt% silicate
71 mantle. In these low-velocity collisions, the impactor loses kinetic energy during its grazing
72 collision with the target, before it is dispersed into a disk around the target. The resulting proto-
73 lunar disk is therefore mainly composed of impactor material. We will call this the “canonical
74 scenario”.

75 When the assumption that no mass is lost is dropped however, the collisional angular momentum is

76 no longer tightly constrained, as lost mass also carries away angular momentum. The total
77 collisional angular momentum can therefore be considerably higher than the final angular
78 momentum in the Earth-Moon system. With this additional degree of freedom, new regions in the
79 collision parameter space become feasible.

80 Apart from the disk mass, another interesting quantity is the origin of the material which ends up in
81 the proto-lunar disk, especially for the silicate part.

82 We call the fraction of target silicate to total silicate material in the disk

83

$$84 \quad f_{\Gamma} = (M_{\text{targ}}^{\text{silc}} / M_{\text{tot}}^{\text{silc}})_{\text{disk}} \quad (1)$$

85

86 where $M_{\text{targ}}^{\text{silc}}$ and $M_{\text{tot}}^{\text{silc}}$ denote the mass of the silicate fraction of the disk derived from the target,
87 and the total disk mass, respectively. If we define a similar target-derived silicate fraction for the
88 post-impact Earth, we can deduce a deviation factor

89

$$90 \quad \delta f_{\Gamma} = (M_{\text{targ}}^{\text{silc}} / M_{\text{tot}}^{\text{silc}})_{\text{disk}} / (M_{\text{targ}}^{\text{silc}} / M_{\text{tot}}^{\text{silc}})_{\text{post-impact Earth}} - 1 \quad (2)$$

91 which directly reflects the compositional similarity between the silicate part of the proto-lunar disk
92 and the silicate part of the post-impact Earth.

93

94 Isotopic measurements show (Wiechert et al., 2001 & Zheng et al., 2012) a strong isotopic
95 similarity between the silicate fractions of today's Moon and Earth. Assuming isotopic
96 heterogeneity of the pre-impact bodies, this suggests that either the material of the bodies mixed
97 during the collision or re-equilibrated their isotopic signatures after the collision. Either scenario is
98 represented by a $\delta f_{\Gamma} \sim 0$ between today's Earth and the Moon. The value of δf_{Γ} right after the
99 impact thus serves as a starting point, from which a re-equilibration mechanism leads to today's
100 value of $\delta f_{\Gamma} \sim 0$.

101 In a typical simulation of the canonical scenario, only about 30% of the disk material and 90% of
102 the material of the post-impact Earth is derived from the target (the proto-Earth) respectively
103 (Canup 2004), yielding a δf_T of -67%.

104

105

106 4. **Results**

107 The new class of collisions presented here falls into the broad regime of slow hit-and-run collisions
108 (Asphaug et al. 2006) with impact velocities between 1.20-1.40 v_{esc} . Hit-and-run occurs up to half
109 the time for collisions with impact velocities in this range. Because of the higher impact velocities
110 in this type of collisions, substantial mass and angular momentum can be lost in the process.

111 Therefore, the initial angular momentum is less constrained and can be considerably higher than the
112 post-impact 1.0-1.1 L_{E-M} angular momentum of the Earth-Moon-system. The higher impact
113 velocities used in these simulations are also encouraged by more recent models of terrestrial planet
114 formation (O'Brien et al. 2006). In hit-and-run collisions, a significant part of the impactor escapes,
115 so that the disk fraction is enriched in target-derived materials compared to the canonical case.

116 Figure 1a shows four consecutive snapshots of such a hit-and-run collision. While the overall
117 characteristics of the collision resemble the canonical scenario, here a considerable part of the
118 impactor is ejected.

119

120 In the new class of giant impact simulations presented in the following paragraphs, for the first time
121 a significantly higher fraction of the material constituting the disk is derived from the Earth's
122 mantle. Table 1 shows a selection of around 60 simulations performed by us. A canonical reference
123 run (cA08) uses initial parameters and conditions similar to those used in the canonical scenario
124 (Canup 2004), successfully reproducing an iron-depleted proto-lunar disk massive enough to form
125 a Moon. For each of our runs, a final Moon mass is calculated using the disk mass and the specific

126 angular momentum (Kokubo, Ida & Makino 2000). We employed three different impactor types
127 with different compositions: chondritic impactors with 70wt% silicates and 30wt% Fe ($v_{\text{esc}} =$
128 9.2km/s, c-runs), iron-rich impactors with 30wt% silicates and 70wt% Fe ($v_{\text{esc}} = 9.3\text{km/s}$, f-runs)
129 and icy impactors with 50wt% water ice, 35wt% silicates and 15wt% Fe ($v_{\text{esc}} = 8.9\text{km/s}$, i-runs).
130 Note that the scaled impact velocity $v_{\text{imp}}/v_{\text{esc}}$ determines the type of collision, as similar-sized
131 collisions in the gravity regime are self-similar (Asphaug 2010, Leinhardt & Stewart 2012). Initial
132 temperatures of the iron cores are between 4000-5000K, for the silicate layers between 1600K-
133 2200K and around 300K for water ice layers. As mentioned before the layers are isentropic and the
134 temperature therefore varies with depth.

135 **5. Discussion**

136 The ratio of target- vs. impactor-derived material that ends up in the proto-lunar disk is mainly
137 defined by the geometry of the collision during the very early phase when the impactor is
138 accelerating target material. This can be seen in Figure 1b, where the particles which later end up in
139 the disk are highlighted in bright colours. In the canonical scenario, the impactor grazes around the
140 target's mantle and is deformed. Due to the low impact velocity, material supposed to end up in
141 orbit around the Earth must not be decelerated too strongly in order to retain enough velocity to stay
142 in orbit. This is only achieved for the parts of the impactor mantle most distant to the point of
143 impact, and some minor part of the target's mantle. But if impact velocity is increased from 1.00
144 ($cA08$) to $1.30 v_{\text{esc}}$ ($cC01$), parts from deeper within the target mantle receive the right amount of
145 energy for orbit insertion, while the outer regions of the target mantle, retain too much velocity and
146 leave the system, thereby removing mass and angular momentum. Both processes work towards
147 increasing the target material fraction in the proto-lunar disk. While in run $cB04$ only $\sim 10\%$ of the
148 initial angular momentum is removed, $\sim 45\%$ are removed in run $cC06$.

149

150 We have found that collisions with an impact angle of $30 - 40^\circ$ and impact velocities of $1.2 - 1.3$

151 v_{esc} are successful in putting significant amounts of target-derived material into orbit, when using
152 differentiated impactors with a chondritic iron/silicates ratio (30wt% Fe, 70wt% silicates) and
153 masses between 0.15-0.20 M_E . Some runs in this regime show an iron excess of $> 5\text{wt}\%$ in the
154 proto-lunar disk and are rejected, as in previous work (Canup 2004). While none of the runs done
155 so far provide a “perfect match” in terms of the constraints from the actual Earth-Moon-system,
156 several simulations come close to that. The best runs coming close to matching the constraints
157 (cC03 and cC06) are obtained using impact angles of 32.5° and 35° and velocities of 1.25 and 1.20
158 v_{esc} , resulting in 54% and 56% of the silicate material deriving from the target, and δf_T thus
159 increasing to -35% and -37% compared to -66% in the reference run of the canonical case. While
160 the satellite masses match well (1.01 and 1.24 M_L), the angular momentum of the runs is somewhat
161 too high (1.28 L_{E-M}). This should, however, be contrasted with other runs, e.g. cB03, where the
162 reduction of the impactor mass to 0.15 M_E results in a similar disk-composition ($\delta f_T = -33\%$), but
163 also a lower Moon mass (0.53 M_L) and a smaller angular momentum of 1.06 L_{E-M} .
164 As collision geometry predominantly determines the fraction of target material in the proto-lunar
165 disk, altering the size of the impactor by density changes should also change the target material
166 fraction in the disk. A denser impactor with the same mass delivers the same momentum, while
167 reducing “spill-over” of impactor material into the disk, as it can be seen in figure 1b. To include
168 such a high density, iron-rich impactor in this study is also motivated by the work of Asphaug 2010,
169 where the population of second-largest bodies in a planet-forming disk becomes slowly enriched in
170 iron through composition-changing hit-and-run collisions. We investigated impactors with 50wt
171 and 70wt% iron core fractions, respectively. With a 0.2 M_E impactor at 30° impact angle and 1.30
172 v_{esc} impact velocity, the target material fraction f_T increases from 57% ($\delta f_T = -34\%$) in the
173 “chondritic” run (cC01), to 64% ($\delta f_T = -28\%$) in the 50wt% iron core run (fA01), and up to 75%
174 ($\delta f_T = -19\%$) in the 70wt% iron core run (fB06). But at the same time, the iron content of the disk
175 increases to values incompatible with lunar data, and also the bound angular momentum increases

176 to unrealistic values. Apparently, reducing the “spill-over” also reduces the lost mass and therefore
177 the lost angular momentum.

178 We also looked into less dense, but still fully differentiated impactors with a composition of 50wt%
179 ice, 35wt% silicate and 15wt% iron, typical for small bodies accreted in regions of the solar system
180 beyond the snow-line. In these runs, the efficiency of putting material into orbit is reduced
181 compared to runs with denser impactors, though the fact that there is less impactor silicate material
182 available to end up in the disk actually raises the target material fraction to 81%, and δf_T to -10% in
183 the case of an $0.2M_E$ impactor hitting at 30° impact angle and $1.30 v_{esc}$ impact velocity (cC01).

184 However, in most runs, the resulting silicate portion of the disk is not massive enough to later form
185 the Moon, although also one run with a silicate portion of $0.73 M_L$ (iA10) was found.

186 A remarkable difference between the new simulations presented here and the canonical model,
187 relevant to the re-equilibration model, is the thermal state of the Earth after the collision. The higher
188 impact velocity leads to stronger shocks and therefore to more intense impact heating. Figure 2
189 shows cuts through the post-impact Earth $\sim 58h$ after the collision, with colour-coded temperature.

190 Temperatures are shown as estimated by ANEOS for the specific energy as it being integrated
191 during the course of a simulation. Note that the values should only be regarded as order of
192 magnitude estimates as heating due to shocks is dependent on how well shocks are resolved, which
193 is resolution dependent. In the canonical case (Figure 2, left panel), only a thin blanket of material
194 raining back from the disk experiences strong heating, while most of the mantle is only moderately
195 heated above the initial average temperature of 2000 K. In the slow “hit-and-run” scenario (Figure
196 2, right panel), the shock is stronger, and a substantial part of the mantle is heated to temperatures
197 above 10'000 K. Beside possible implications for the early history of the Earth, this also constitutes
198 a different starting point for the re-equilibration model (Pahlevan & Stevenson 2007). While in the
199 canonical model, the thin hot blanket may inhibit convection within the Earth, and thereby isotopic
200 re-equilibration at early stages, the much thicker hot layer which extends deep into the mantle in

201 our model probably simplifies exchange of material between the deep interior of the post-impact
202 Earth and the hot silicate vapour atmosphere. It is important to note, that the post-impact
203 temperatures depend not only on the magnitude of shock heating experienced during the collision,
204 but also on the initial temperature profiles of the pre-impact bodies and the numerical method
205 employed. The absolute temperatures obtained in this study therefore should only be used to
206 qualitatively compare the effect of different impact parameters on the impact heating. Also note that
207 our model neglects strength and therefore leads to a slightly changed attenuation of the shock wave
208 and therefore to a changed shock heating.

209

210 Our results not only relax the required efficiency of re-equilibration by starting with a disk with a
211 higher target material fraction, but the resulting thermodynamical state might actually create a more
212 favourable starting point for re-equilibration.

213

214 Another important difference to the canonical scenario is the dynamical state of the proto-lunar
215 disk. In both scenarios, material is ejected on ballistic trajectories after impact and forms an arm-
216 like structure. Angular momentum is transferred from the inner to the outer part, thus circularising
217 the orbit of the outer part of the arm while the inner part re-impacts the Earth. In the “hit-and-run”
218 scenario, this arm structure persists for a shorter time compared to the canonical case, transferring
219 less angular momentum and leaving the material on more eccentric orbits. The dynamical evolution
220 of such an eccentric disk and the consequences for Moon formation have yet to be studied. Also, the
221 effects of pre-impact rotation of both the target and the impactor will have to be studied in future
222 work.

223

224 5. **Conclusions**

225 In summary, our new giant impact scenario based on a “hit-and-run” collision at higher impact

226 velocity ($1.20 - 1.25 v_{\text{esc}}$) and a steeper impact angle ($30 - 35^\circ$) than assumed in the canonical
227 scenario provides an alternative scenario for the giant impact, with a different starting point for
228 lunar accretion in the post-impact debris disk. The thermal state of this disk is considerably hotter
229 compared to the canonical scenario.

230

231 **6. Acknowledgements**

232 We thank Maria Schönbachler, Kaveh Pahlevan and Vera Fernandes for discussions and Jay Melosh
233 for providing us with the M-ANEOS package. Andreas Reufer and Matthias M. M. Meier were
234 both supported by the Swiss National Science Foundation. All calculations were performed on the
235 ISIS2 cluster at University of Bern.

236

237 *Asphaug, E., Agnor, C. B., Williams, Q., 2006, Hit-and-run planetary collisions, Nature 439,*
238 *pp.155-160*

239 *Asphaug, E., 2010, Similar-sized collisions and the diversity of Planets, Chemie der Erde, vol. 70,*
240 *pp. 199*

241 [Benz, W., Slattery, W. L., Cameron, A. G. W.](#), 1986, The origin of the Moon and the single impact
242 hypothesis I, *Icarus* 66, pp.515-535,

243 [Benz, W., Slattery, W. L., Cameron, A. G. W.](#), 1985, *The origin of the Moon and the single impact*
244 *hypothesis II*, *Bulletin of the American Astronomical Society* 17, p.726

245 Benz, W., Cameron, A. G. W., Melosh, H. J., 1989, The origin of the Moon and the single impact
246 hypothesis III, *Icarus* 81, pp.113-131

247 Cameron, A.G.W., Ward, W. R., 1976, The origin of the Moon, Abstracts of the Lunar and Planetary
248 Science Conference

249 Canup, R.M. & Asphaug, E., 2001, Origin of the Moon in a giant impact near the end of the Earth's
250 formation, *Nature* 412, pp. 708,

251 Canup, R.M., Ward, W. R., Cameron, A. G. W., 2001, A scaling law for satellite-forming impacts,
252 Icarus 150, pp.288-296,

253 Canup, R.M., 2004, Simulations of a late lunar-forming impact, Icarus 168, pp.433-456

254 Kokubo, E., Ida, S. & Makino J., 2000, Evolution of a Circumterrestrial Disk and Formation of a
255 Single Moon, Icarus 148, pp. 419

256 Melosh, H.J., 2007, A hydrocode equation of state for SiO₂, Meteoritics & Planetary Science, vol.
257 42, pp. 2079

258 Leinhardt, Z.M. & Stewart, S.T., 2012, Scaling Laws for Collisions between Gravity Dominated
259 Bodies, Astrophysical Journal, vol. 745, pp. 79

260 Monaghan, J. J., 1992, Smoothed particle hydrodynamics, Annual review of astronomy and
261 astrophysics. Vol. 30, p. 543-574

262 O'Brien, D. P., Morbidelli, A, Levison, H. F., 2006, Terrestrial planet formation with strong
263 dynamical friction, Icarus 184, pp. 39

264 Pahlevan, K. & Stevenson D.J., 2007, Equilibration in the aftermath of the lunar-forming giant
265 impact, EPSL, vol. 262, pp. 438

266 Reufer, A., 2011, Collisions in planetary systems, PhD thesis, Universität Bern

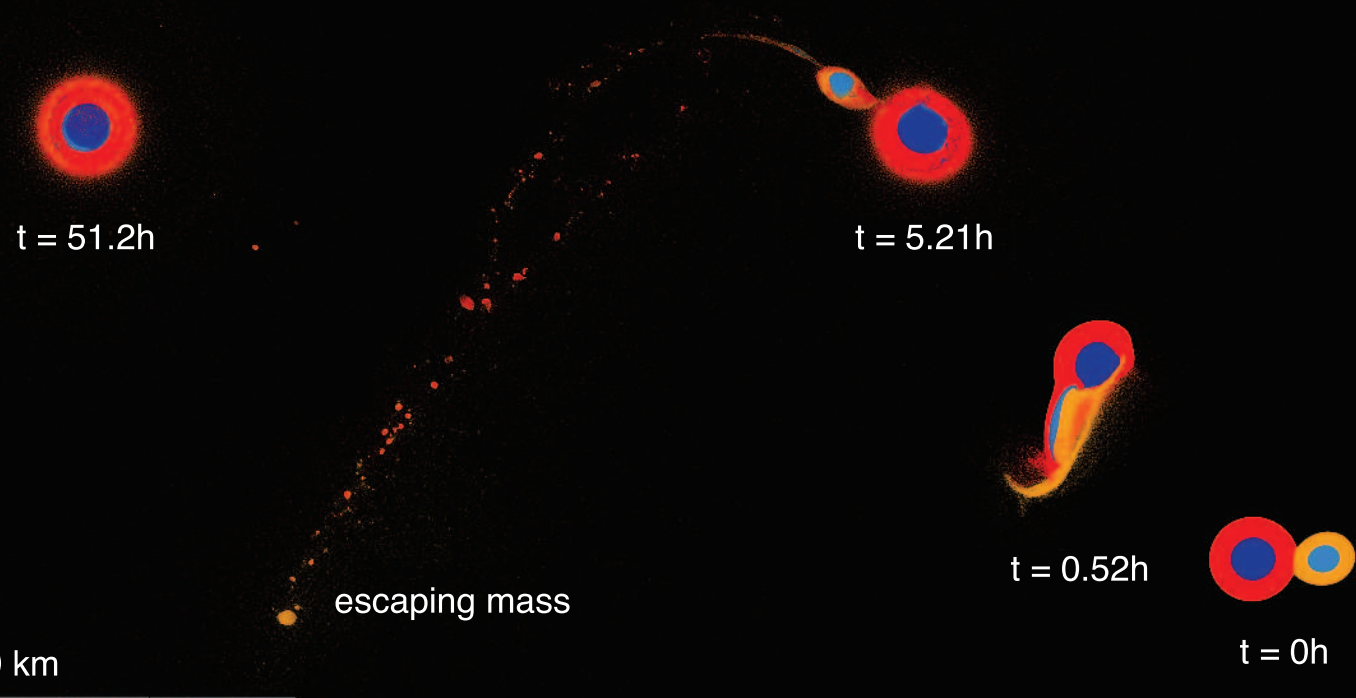
267 Thompson, S.L. & Lauson, H.S., 1972, Improvements in the CHART D radiation — hydrodynamic
268 code III: revised analytic equations of state. Technical Report, SC-RR-71-0714

269 Wiechert, U., Halliday, A. N., Lee, D.-C., Snyder, G. A., Taylor, L. A., Rumble, D., 2001, *Oxygen*
270 *Isotopes and the Moon-forming Giant Impact*, Nature 294, pp.345,

271 Zhang J., Dauphas N., Davis A. M., Leya I. and Fedkin A., 2012, *The proto-Earth as a significant*
272 *source of lunar material*, Nature Geoscience 5, 251–255,

Figure 1

a



b

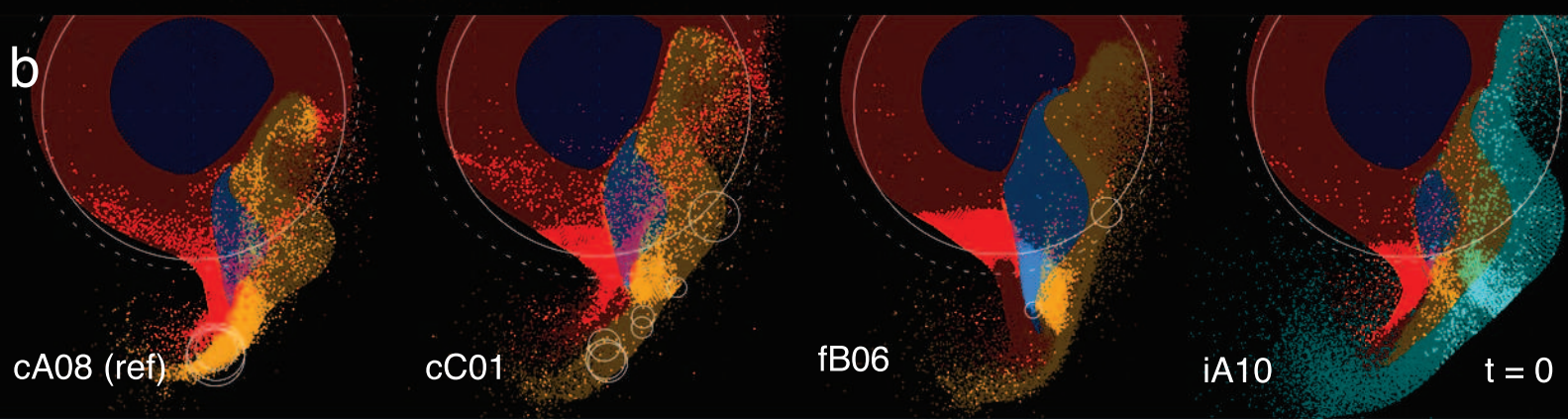


Figure 2

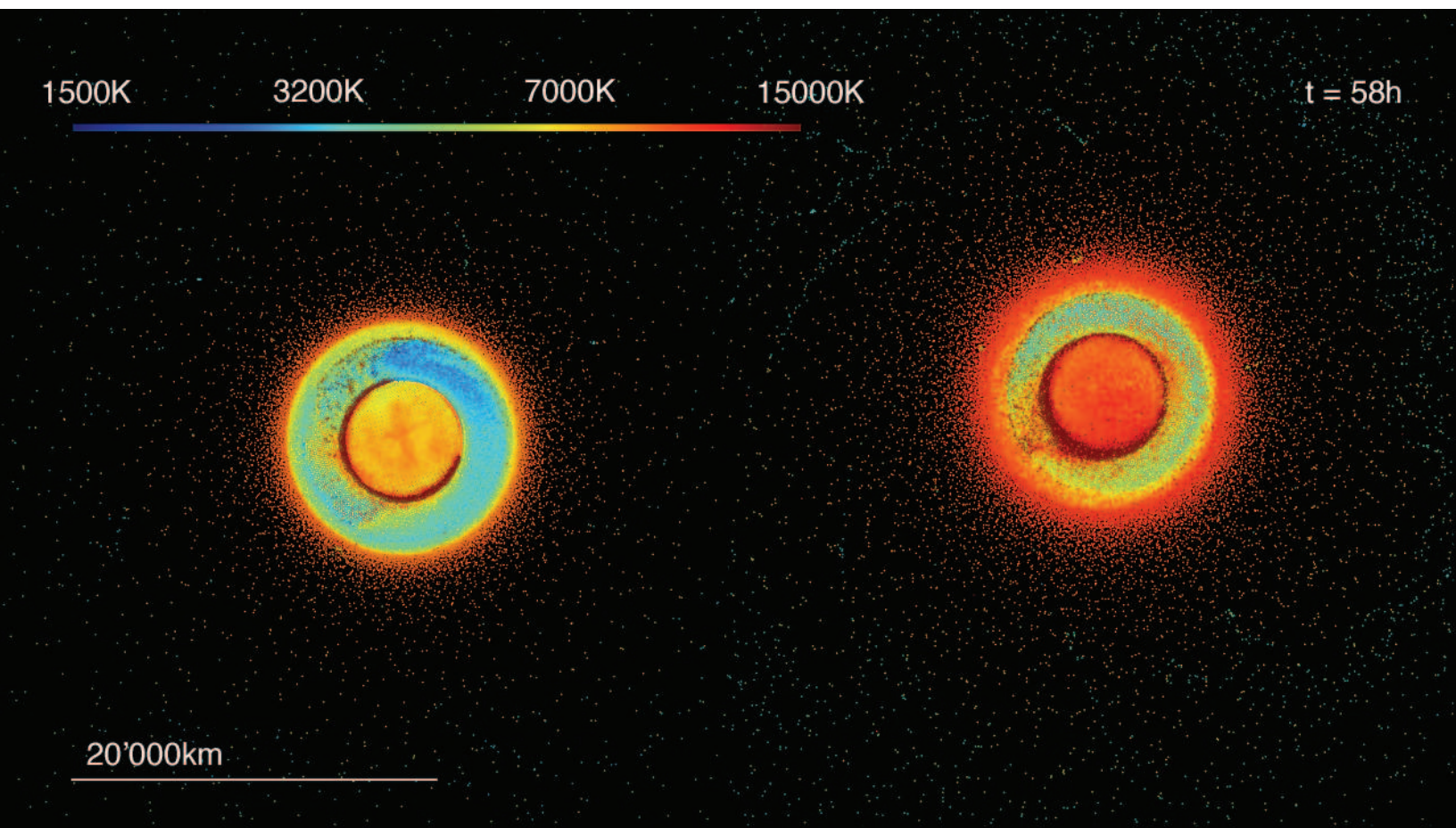


Figure 1a: Five snapshots from the 30° impact angle and $1.30v_{\text{esc}}$ impact velocity case (cC06) showing cuts through the impact plane. Colour coded is the type and origin of the material. Dark and light blue indicate target and impactor iron; Red and orange show corresponding silicate material. The far right shows the situation at the time of impact. At 0.52h, it can be seen how the impactor ploughs deep through the target's mantle and pushes considerable amount of target material into orbit. A spiral arm of material forms and gravitationally collapses into fragments. The outer portions of the arm mainly consist of impactor silicates and escapes due to having retained a velocity well above escape velocity. The silicate fragments further inward are stronger decelerated and enter eccentric orbits around the target. The impactor's iron core also loses much of its angular momentum to the outer parts of the spiral arm and re-impacts the proto-Earth.

Figure 1b: The origin of the disk material highlighted, half a collisional timescale ($(R_{\text{imp}} + R_{\text{tar}}) / v_{\text{imp}}$) after impact. In the grazing reference case (cA08), the majority of the proto-lunar disk originates from a spill-over of the impactor. In the head-on cases (cC01, fB06, iA10), much more material comes from the target mantle, being pushed out into orbit by the impactor core. Colours are identical to figure 1. Turquoise on the right shows water ice for the icy impactor case iA10.

Figure 2: Comparing post-impact temperatures of the proto-Earth between the grazing reference simulation left (cA08) and the head-on case on the right (cC06). Colour coded is temperature in K in logged scale. The initial average temperature before the impact inside the target mantle is $\sim 2000\text{K}$.

Table 1

run	M_{tar} [M_E]	M_{imp} [M_E]	θ [$^\circ$]	v_{imp} [v_{esc}]	impactor [wt% Fe/SiO ₂ /H ₂ O]	δf_T	f_T	M_{moon} [M_L]	L_D [L_{E-M}]	M_D [M_L]			L_{bound} [L_{E-M}]	L_{imp} [L_{E-M}]
										SiO ₂	Fe	H ₂ O		
cA01	0.90	0.10	30.0	1.35		-18%	77%	0.03	0.02	0.12	0.00	0.00	0.67	1.04
cA02	0.90	0.10	32.5	1.30		-26%	69%	0.05	0.02	0.13	0.01	0.00	0.70	1.07
cA03	0.90	0.10	32.5	1.50		-35%	61%	0.10	0.03	0.18	0.02	0.00	0.57	1.24
cA04	0.90	0.10	35.0	1.30		-36%	60%	0.16	0.05	0.23	0.06	0.00	0.68	1.14
cA05	0.90	0.10	35.0	1.35		-36%	61%	0.20	0.06	0.26	0.07	0.00	0.64	1.19
cA06	0.90	0.10	35.0	2.00	30 / 70 / 0	-31%	68%	0.02	0.01	0.09	0.01	0.00	0.33	1.76
cA07	0.90	0.10	45.0	1.00		-49%	46%	0.53	0.14	0.81	0.00	0.00	0.95	1.08
cA08	0.90	0.10	48.0	1.00		-66%	31%	1.50	0.28	1.27	0.00	0.00	0.97	1.14
cA09	0.90	0.10	50.0	1.00		-66%	32%	0.68	0.15	0.80	0.02	0.00	0.94	1.18
cA10	0.90	0.10	53.0	1.00		-75%	23%	0.89	0.21	0.96	0.15	0.00	0.96	1.23
cB01	0.90	0.15	32.5	1.15		-41%	53%	0.10	0.03	0.23	0.00	0.00	1.06	1.49
cB02	0.90	0.15	35.0	1.15	30 / 70 / 0	-35%	58%	0.23	0.06	0.37	0.01	0.00	1.10	1.59
cB03	0.90	0.15	35.0	1.20		-33%	60%	0.53	0.15	0.86	0.05	0.00	1.06	1.66
cB04	0.90	0.15	40.0	1.10		-41%	53%	1.20	0.27	1.41	0.04	0.00	1.16	1.71
cC01	0.90	0.20	30.0	1.30		-34%	57%	0.52	0.16	1.00	0.06	0.00	1.20	2.18
cC02	0.90	0.20	32.5	1.20		-30%	61%	0.90	0.27	1.63	0.03	0.00	1.40	2.16
cC03	0.90	0.20	32.5	1.25		-37%	54%	1.01	0.27	1.51	0.06	0.00	1.27	2.25
cC04	0.90	0.20	32.5	1.30		-32%	58%	1.12	0.27	1.39	0.14	0.00	1.30	2.34
cC05	0.90	0.20	35.0	1.15	30 / 70 / 0	-36%	54%	1.32	0.35	1.98	0.03	0.00	1.46	2.21
cC06	0.90	0.20	35.0	1.20		-35%	56%	1.24	0.29	1.60	0.01	0.00	1.28	2.31
cC07	0.90	0.20	45.0	1.00		-54%	39%	1.30	0.31	1.61	0.06	0.00	1.74	2.37
cC08	0.90	0.20	50.0	1.00		-76%	20%	3.16	0.65	2.84	0.37	0.00	2.02	2.57
fA01	0.90	0.20	30.0	1.30		-28%	64%	0.95	0.29	1.50	0.37	0.00	1.40	2.16
fA02	0.90	0.20	35.0	1.20		-28%	63%	1.18	0.26	1.20	0.13	0.00	1.55	2.28
fA03	0.90	0.20	32.5	1.25	50 / 50 / 0	-31%	62%	1.16	0.29	1.41	0.25	0.00	1.48	2.23
fA04	0.90	0.20	35.0	1.25		-24%	67%	1.33	0.29	1.22	0.26	0.00	1.57	2.38
fA05	0.90	0.20	40.0	1.10		-33%	59%	1.17	0.29	1.56	0.09	0.00	1.68	2.34
fB01	0.90	0.10	30.0	1.35		-23%	74%	0.03	0.02	0.08	0.05	0.00	0.74	1.01
fB02	0.90	0.10	35.0	1.30		-28%	69%	0.38	0.11	0.37	0.30	0.00	0.78	1.12
fB03	0.90	0.10	40.0	1.10		-25%	73%	0.31	0.10	0.46	0.16	0.00	0.85	1.06
fB04	0.90	0.10	45.0	1.00	70 / 30 / 0	-19%	78%	0.39	0.11	0.59	0.12	0.00	0.89	1.06
fB05	0.90	0.10	48.0	1.00		-33%	64%	0.72	0.18	0.51	0.54	0.00	0.97	1.12
fB06	0.90	0.20	30.0	1.30		-19%	75%	1.48	0.37	1.40	0.68	0.00	1.47	2.13
fB07	0.90	0.20	30.0	1.35		-18%	76%	1.63	0.38	1.38	0.71	0.00	1.48	2.21

Table 1.: Simulation results. Note that L_D and M_{moon} estimated according to (Kokubo 2000) considers all disk material, including any present iron and water ice.

run	M_{tar} [M_E]	M_{imp} [M_E]	θ [$^\circ$]	v_{imp} [v_{esc}]	impactor [wt% Fe/SiO ₂ /H ₂ O]	δf_T	f_T	M_{moon} [M_L]	L_D [L_{E-M}]	M_D [M_L]			L_{bound} [L_{E-M}]	L_{imp} [L_{E-M}]
										SiO ₂	Fe	H ₂ O		
iA01	0.90	0.20	15.0	1.50		-6%	84%	-0.13	0.02	0.21	0.00	0.08	0.75	1.35
iA02	0.90	0.20	25.0	1.30		-26%	66%	0.17	0.09	0.47	0.00	0.19	1.12	1.92
iA03	0.90	0.20	25.0	1.35		-23%	69%	0.15	0.08	0.41	0.00	0.18	1.08	1.99
iA04	0.90	0.20	25.0	1.50		-16%	76%	0.07	0.07	0.47	0.00	0.16	0.92	2.21
iA05	0.90	0.20	25.0	1.75		-24%	71%	0.17	0.07	0.38	0.01	0.11	0.60	2.58
iA06	0.90	0.20	30.0	1.00		-20%	71%	0.20	0.10	0.20	0.00	0.52	1.28	1.74
iA07	0.90	0.20	30.0	1.15		-52%	43%	0.76	0.21	0.62	0.00	0.65	1.36	2.01
iA08	0.90	0.20	30.0	1.20		-62%	34%	0.91	0.23	0.75	0.00	0.59	1.35	2.09
iA09	0.90	0.20	30.0	1.25		-20%	72%	0.36	0.11	0.33	0.00	0.35	1.15	2.18
iA10	0.90	0.20	30.0	1.30		-10%	81%	0.60	0.17	0.73	0.00	0.33	1.12	2.27
iA11	0.90	0.20	30.0	1.32		-14%	78%	0.26	0.09	0.26	0.00	0.37	1.00	2.30
iA12	0.90	0.20	30.0	1.35		-10%	82%	0.32	0.11	0.45	0.00	0.30	0.96	2.36
iA13	0.90	0.20	32.5	1.25		-15%	77%	0.71	0.19	0.56	0.00	0.56	1.01	2.34
iA14	0.90	0.20	32.5	1.30		-23%	70%	1.08	0.23	0.79	0.00	0.36	1.09	2.44
iA15	0.90	0.20	32.5	1.35	15 / 35 / 50	-54%	42%	2.19	0.45	1.50	0.26	0.48	1.06	2.53
iA16	0.90	0.20	35.0	1.00		-60%	36%	1.35	0.32	0.70	0.00	1.03	1.51	2.00
iA17	0.90	0.20	35.0	1.10		-30%	63%	1.61	0.37	0.92	0.00	1.07	1.42	2.20
iA18	0.90	0.20	35.0	1.15		-60%	36%	3.03	0.59	1.50	0.00	1.23	1.57	2.30
iA19	0.90	0.20	35.0	1.20		-60%	36%	2.89	0.52	1.23	0.00	0.95	1.55	2.40
iA20	0.90	0.20	35.0	1.25		-56%	40%	2.26	0.50	1.73	0.16	0.74	1.23	2.50
iA21	0.90	0.20	35.0	1.30		3%	98%	-0.01	0.00	0.02	0.00	0.02	0.48	2.60
iA22	0.90	0.20	40.0	1.15		-70%	27%	8.14	1.39	2.80	0.80	1.97	2.03	2.58
iA23	0.90	0.20	45.0	1.00		-67%	30%	2.04	0.49	1.28	0.01	1.39	1.71	2.47
iA24	0.90	0.20	45.0	1.15		-61%	37%	0.09	0.04	0.09	0.00	0.19	1.14	2.84
iA25	0.90	0.20	45.0	1.20		-1%	97%	0.01	0.01	0.03	0.00	0.05	0.35	2.96
iA26	0.90	0.20	45.0	1.25		-10%	89%	0.01	0.01	0.03	0.00	0.04	0.35	3.08
iA27	0.90	0.20	60.0	1.00		-73%	24%	0.96	0.28	0.75	0.01	0.99	1.41	3.02
iA28	0.90	0.20	60.0	1.15		0%	100%	0.00	0.00	0.01	0.00	0.02	0.16	3.48

Table 1. (continued)